The effect of the anomeric configuration on the micellization of hexadecylmaltoside surfactants

Johan Larsson,[a] Adrian Sanchez-Fernandez,[b] Najet Mahmoudi,[c] Lester C. Barnsley,[d] Marie Wahlgren,[b,e] Tommy Nylander,[a,f] Stefan Ulvenlund[b,e]

[a]Physical Chemistry, Department Chemistry, Lund University, Box 124, 221 00 Lund, Sweden.

[b]Food Technology, Engineering and Nutrition, Lund University, Box 124, 221 00 Lund, Sweden.

[c]ISIS Spallation Source, STFC, Rutherford Appleton Laboratory, Didcot, UK.

[d]Jülich Centre for Neutron Science (JCNS) at Heinz Maier-Leibnitz Zentrum (MLZ), Forschungszentrum Jülich GmbH, Lichtenbergstr. 1, 85748 Garching, Germany.

[e]Enza Biotech AB, Scheelevägen 22, 22363 Lund, Sweden.

[f]NanoLund, Lund University, Lund, Sweden

The self-assembly of the two anomeric forms of n-hexadecyl-D-maltopyranoside (denoted α-$C_{16}G_2$ and β-$C_{16}G_2$) has been studied in dilute aqueous solution by means of surface tension measurements, scattering methods (dynamic light scattering, static light scattering, and small-angle X-ray and neutron scattering) and cryo-transmission electron microscopy at different surfactant concentrations and temperatures. Surface tension measurements demonstrates differences in the surfactant adsorption at the air-water interface, where α-$C_{16}G_2$ shows a lower

CMC than β-$C_{16}G_2$. Similarly, micelle morphology was found to depend on anomerism, concentration and temperature. β-$C_{16}G_2$ preferentially form very elongated micelles with large persistence lengths, whereas α-$C_{16}G_2$ assembles into smaller micelles for which the structure varies with concentration and temperature. The differences between the two surfactant anomers in terms of self-assembly can be attributed to the interaction between neighboring headgroups. Specifically, β-$C_{16}G_2$ allows for a closer packing in the palisade layer, hence reducing the micelle curvature and promoting the formation of more elongated micelles. Strong intermolecular headgroup interactions may also account for the observed rigidity of the micelles.

Introduction

Non-ionic surfactants are key ingredients in many types of consumer goods, for instance formulated products in pharmaceutics, cosmetics and personal care. However, the majority of these surfactants are currently produced from non-renewable resources, for example ethoxylated surfactants which are synthesized from fossil based materials. The search for new sustainable components, as well as the characterization of existing ones, is the subject of substantial research efforts. Since the late 1990s, alkylglycosides are extensively used in formulated products, [1-4] since they are recognized as environmentally friendly and non-toxic materials, while still being highly functional and cost-efficient. Furthermore, these surfactants have been implemented in high-end niche applications, such as the solubilization and stabilization of membrane proteins.[5] In spite of their extensive and varied commercial use, alkylglycosides are still not fully understood in terms of their complex self-assembly and interfacial behavior, limiting the exploitation of these in new applications. In contrast to alkylglycosides, ethoxylated surfactants are understood in great detail in terms of the influence of surfactant structure (length of alkyl chain and degree of headgroup polymerization) on general phase behavior (concentration and

temperature dependence),[6-8] micelle formation (CMC and micelle morphology),[9-10] and adsorption to various interfaces.[11] This knowledge has been shown to be crucial for the design of formulated products containing this type of surfactants. Our ultimate aim is to build the same level of knowledge for alkylglycosides.

In line with this ambition, previous investigations have been focused on the study of the self-assembly of sugar-based surfactants with different tail length and sugar units in the headgroup. Some key results from previous studies are summarized in Table 1

Table 1. CMC and morphology of alkylglycoside micelles (glucoside – G_1; maltoside – G_2) in aqueous solutions. All of the reported morphologies were determined at room temperature, with the exception of β-$C_{14}G_2$, which was measured at 50 ˚C.

Surfactant	CMC / mM	Micelle morphology
β-C_7G_1	71.8[12]	Short cylinder.[12]
β-C_8G_1	23.6[12]	Prolate ellipsoid,[13-14] cylinder.[12, 15]
α-C_8G_1	17.1[14]	Prolate ellipsoid.[14]
β-C_9G_1	6.9[16]	Prolate ellipsoid,[13, 17] cylinder.[12, 16]
β-$C_{10}G_1$	2.2[17]	Network of thread-like micelles.[17]
β-C_8G_2	19.1[18]	Sphere.[18]
β-$C_{10}G_2$	2.2[19]	Oblate ellipsoid,[13] prolate ellipsoid.[20]
α-$C_{12}G_2$	0.15[21]	Sphere.[21]
β-$C_{12}G_2$	0.20[21]	Oblate ellipsoid,[13, 21-24] prolate ellipsoid.[20, 25]
β-$C_{14}G_2$	0.014[26]	Cylinder.[26]

When rationalizing micelle morphology based on molecular structure, the simple concept of critical packing parameter (CPP) has proved to be a valuable qualitative tool. CPP is defined as $v/(a_0 l_c)$, where v is the volume of the hydrophobic moiety, l_c is the critical length of the surfactant

tail, and a_0 is the area of the headgroup-tail interface of the monomer.[27] For ethoxylated surfactants the morphology of the micellar assemblies, as well as their dependence on temperature, follow the expected trends, e.g. surfactants with long hydrophobic tail and/or short head-groups form more elongated aggregates (1/3<CPP<1/2), whereas shorter tail and longer headgroup promote spherical or quasi-spherical micelles (CPP=1/3). Similarly, micelle formation of alkylglucoside surfactants (i.e. G_1 species) follow the trend expected from CPP arguments, namely that increasing length of the alkyl chain leads to a shift from spherical symmetry to ellipsoidal to cylindrical structures (Table 1). From the meagre information available, α/β-anomerism does not seem to have a major influence on the micellar structures for the glucosides.[28] For alkylmaltoside surfactants (G_2 species), increasing alkyl chain length from C_8 to C_{14} gives several morphology transitions, as the formation of spherical, prolate, oblate and cylindrical aggregates has been reported.[20, 26] The micelle morphology seems also to be temperature dependent for these surfactants. For example, smaller aggregates are formed in the case of $C_{12}G_2$ when temperature increases, whilst $C_{14}G_2$ micelles increases in size at higher temperatures. Furthermore, headgroup anomerism seems to have an influence in micelle morphology, as judged from the data on the α- and β-anomers of dodecylmaltoside ($C_{12}G_2$).[20-21]

From the existing data, it is clear that the self-assembly of alkylmaltoside surfactants is complex and not readily rationalized from the behavior of other non-ionic surfactants. When discussing differences in morphology and dynamics between ethoxylate and alkylglycoside micelles, it is critical to consider the fundamental differences between the headgroups. The headgroups in the first case consist of freely jointed chains, in which the intermolecular interactions are dominated by hydrogen bonding with the solvent, where the ether units act as hydrogen bond acceptors. This limits the opportunities for strong specific interactions between

headgroups.[10] The alkylglycoside surfactant headgroups, on the other hand, consist of rigid subunits that can be oriented in such a way that different types of (attractive) intermolecular interactions become important. The most obvious type of interaction is hydrogen bonding, as elsewhere reported for other sugar-based materials (e.g. cellulose). For micelles in aqueous solution, the formation of hydrogen bonds between headgroups competes with hydrogen bonding between glucose units and water molecules, as the glucose unit can act as both hydrogen bond donor and acceptor. However, NMR T_2 relaxation experiments suggest that hydrogen bonding between OH groups of glucose moieties is of critical importance when describing alkylglycoside micelles.[29] Similarly, intermolecular hydrogen bonds in foam lamellae have been proposed as an explanation for the unusually good foaming properties of alkylglycosides.[30] Also, the importance of hydrogen bonding with neighboring water molecules, combined with the rapid proton exchange between glucose hydroxyl groups and water, is demonstrated by the sometimes dramatic difference in behavior of alkylglycosides between H_2O and D_2O.[16, 26, 31]

In addition to their propensity to form hydrogen bonds, the glucose units in alkylglycosides are also weakly amphiphilic. This property is often overlooked, but manifests itself in the complexing ability of cyclodextrins, in which the hydrophobic cavity may act as a host to non-polar guest molecules [32-33] More recently, the amphiphilicity of glucose residues has also been proposed as an explanation of the low solubility of cellulose in water ("The Lindman Hypothesis").[34-35] It would seem likely that the same amphiphilicity, and the resulting hydrophobic interactions between adjacent head-groups, may influence the properties of alkylglycoside surfactants in the micellar state.

In the present study, we investigate how the headgroup interaction affects the assembly of the alkylglycoside in bulk solution and at interfaces by comparing the α- and β-anomer of n-

hexadecylmaltoside (α-$C_{16}G_2$ and β-$C_{16}G_2$). The interfacial behavior of the surfactants has been investigated by means of surface tension, and the bulk behavior has been explored using dynamic light scattering (DLS), static light scattering (SLS), small-angle X-ray scattering (SAXS), small-angle neutron scattering (SANS) and cryo-transmission electron microscopy (cryo-TEM). Apart from the fundamental interest, α-$C_{16}G_2$ and β-$C_{16}G_2$ are also interesting from an applied point of view because of their long alkyl chain. Surfactants with long alkyl chains tend to be good solubilizers, efficient emulsifiers and thickening agents. However, the self-assembly of long-chain alkylglycosides are almost entirely unknown and in particular the effect of headgroup orientation has not been studied before.

Experimental section

Materials and Sample Preparation. n-Hexadecyl-α-D-Maltopyranoside (α-$C_{16}G_2$; Figure 1) was purchased from Ramidus (Lund, Sweden) and had a purity of >97%. The β-anomer of the same compound (β-$C_{16}G_2$; Figure 1), was purchased from Anatrace Inc. (Maumee, Ohio) and was of Anagrade quality. According to the supplier, the purity of this product is ≥97%, out of which ≥95% is the β-$C_{16}G_2$ anomer. As a part of the present study, the purity of the materials claimed by the suppliers was verified by HPLC and mass spectroscopic analyses. The results from the characterization are presented in the Supporting information. Samples were prepared by mixing α- or β-$C_{16}G_2$ with the desired solvent under agitation with magnetic stirring in water bath at 45 °C. H_2O used in this work was of MilliQ-quality, and D_2O was purchased from Sigma Aldrich (Darmstadt, Germany) and had an isotropic purity of 99.9%.

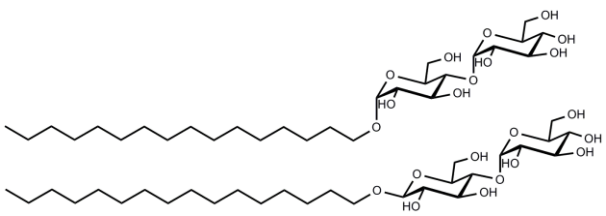

Figure 1 Molecular structure of α-C16G2 (top) and β-C16G2 (bottom).

The Krafft temperature of both α-$C_{16}G_2$ and β-$C_{16}G_2$ was estimated to be between 25 and 35 ˚C through visual inspection, and therefore above room temperature. Thus, the solutions are physically unstable and prone to precipitation at room temperature. The rate of precipitation was found to depend on concentration. At concentrations above 10 mM, precipitate was observed after about 1 h at 25°C, while at 1 µM, samples were found to be stable overnight. Thus, all measurements for high surfactant concentration conducted at temperatures below the Krafft point were performed within one hour after preparation, in order to avoid confounding effects stemming from precipitation.

Methods

Tensiometry. A Du Noüy ring tensiometer from Krüss (Hamburg, Germany) was used to determine the surface tension of α- and β-$C_{16}G_2$ solutions at ambient temperature as a function of surfactant concentration. The Du Noüy ring was made of platinum. 100 ml surfactant samples were prepared in a narrow beaker with a radius of 2.5 cm. As will be discussed in more detail in the Results section, the ratio of surface area to volume of the vessel was found to be critical to get reliable results, due to the low CMC of the surfactant.

The surface tension was measured as a function of time, until a stable value was reached. This stable value was recorded as the equilibrium surface tension value. The time required to reach stable readings for samples with concentrations around and below the CMC was found to be 90±15 minutes, but the time required for equilibration decreased significantly with concentration. Thus, at concentrations more than two orders of magnitude higher than the CMC, stable readings were achieved in less than a minute. Duplicate measurements were performed for each concentration.

Dynamic Light Scattering (DLS). The effective hydrodynamic radius (R_H) of the micelles were determined using a Zetasizer Nano-ZS (Malvern Instruments Ltd., Worshestershire, UK) with non-invasive backscatter (NIBS) technology operating with a scattering angle of 173°. The light source was a 4 mW He-Ne laser with a wave length of 632.8 nm. For each experiment, 0.5 ml of sample was transferred to PMMA semi-micro disposable cuvettes purchased from BRAND GmbH (Wertheim, Germany). For measurements above 70 °C, quartz glass SUPRASIL cuvettes from Hellma Analytics (Müllheim, Germany) were used.

The correlation function data did not reveal any bimodality under the applied experimental conditions. Thus, DLS data were analyzed using the cumulant method implemented in the Malvern software supplied with the instrument, were a single exponential function provided a good fit to the experimental data. Results from these measurements were presented as hydrodynamic radius.

Static Light Scattering (SLS). For the SLS experiments an ALV/DLS/SLS-5022F, CGF-8F-based compact goniometer system from ALV GmbH (Langen, Germany) was used. The laser source was a 22 mW He-Ne laser with a wavelength of 632.8 nm, and an automatic attenuator was used to vary the intensity. The temperature was controlled by a F32 Julabo heating circulator with an accuracy of ±0.01 °C. Measurements were made at 24 angles with corresponding Q-values between 5.72×10^{-4} $Å^{-1}$ to 2.52×10^{-3} $Å^{-1}$, where Q is the scattering momentum transfer ($Q=4\pi\sin\theta/\lambda$). For every angle, 3 measurements at 40 ˚C were performed and averaged. Data were reduced, normalized and scaled to match the neutron scattering excess of the hydrogenated surfactant in D_2O. Output data were the angular-dependent scattered intensity *versus* momentum transfer Q.

Small-Angle X-ray and Neutron Scattering. Small-angle X-ray scattering (SAXS) experiments were performed on beam line BM29 at the European Synchrotron Radiation Facility (Grenoble, France).[36] The wavelength was 0.99 Å and the distance from sample to the detector was 2.867 m, resulting in a Q-range of 0.0040 – 0.49 $Å^{-1}$. Measurements were performed at 25, 40 and 50 °C using the temperature-controlled sample stage. The acquisition time was 10 seconds (1 second exposure, 10 frames) per sample and frames affected by radiation damage were removed. The absolute scale for the scattered intensity was obtained using the standard protocols of the beamline.[37]

SANS measurements were performed on the KWS-1 instrument at the Heinz Maier-Leibnitz Zentrum (Garching, Germany) and on SANS2D instrument at the ISIS Neutron and Muon Source (Didcot, UK).[38-40] On KWS-1, the wavelength of the neutrons was 7 Å and 3 different sample-to-detector distances were used (2 m, 8 m and 20 m), yielding to a combined Q-range of 0.0015-0.3 $Å^{-1}$. For the experiment on SANS2d, the front and rear detector were placed at 5 m and 12 m from the sample position respectively. Neutrons with wavelengths between 1.75 and 12.5 Å were used, providing a combined Q-range of 0.0016-0.5 $Å^{-1}$. In both experiments, samples were loaded in quartz cuvettes with a path length of 2 mm for D_2O and 1 mm for H_2O and measured at 50 ˚C. Data were corrected for detector efficiency, background noise, sample transmission and scattering from an empty cell using the standard protocols of each beamline. Solvent contribution was subtracted from the scattering of the samples. The output data were absolute intensity ($I(Q)$, cm^{-1}) versus momentum transfer (Q, $Å^{-1}$).[38]

Small-angle scattering data were analyzed using form factor models that appropriately describe the scattering from the micelles in the particular system. These models were implemented in SasView 4.2.2. and were fitted to the experimental data using a Levenberg–Marquardt

algorithm.[41] The X-ray and neutron scattering length density (SLD) of each component of the system was calculated from the scattering length of the unit (b) and the volume it occupies (V_m). These values are presented in Table 2.

Table 2 Volume, scattering length and scattering length density for X-rays and neutrons of each constituent of the system.

Unit	V_m / Å^3	b X-ray / fm	SLD X-ray / 10^{-6} Å^{-2}	b neutron / fm	SLD neutron / 10^{-6} Å^{-2}
α-/β-G_2	368[a]	510	13.9	65.1	1.77
$C_{16}H_{33}$	431[b]	363	8.44	-17.1	-0.40
H_2O	29.9[c]	28.2	9.42	-1.68	-0.56
D_2O	29.9[c]	-	-	19.15	6.40

[a]The molecular volume of the maltoside unit was calculated from the physical density of maltose.

[b]The molecular volume of the hydrophobic tail of the surfactant has been calculated using the Tanford equation.[42]

[c]The molecular volume of H_2O and D_2O have been calculated from the physical density of those at 25 ˚C.

The high-Q expansion of X-ray and neutron data (Q > 0.006 Å^{-1}) were fitted using core-shell cylinder model that satisfactorily describes the cross-section of elongated micelles (elongation > 10 times the radius of the cross-section).[43] For shorter micelles (elongation ≤ 10 times the radius of the cross-section), a core-shell ellipsoid model was found to be more appropriate to model the experimental scattering data. The fitting approach was performed as follows: the micelle core SLD and solvent SLD were fixed to the calculated values (Table 2). The structural parameters (L_{core} – core length, r_{core} – core radius, t_{shell} – shell thickness; for the prolate ellipsoid model L_{core} corresponds to twice the size of the core along the rotational axis and r_{core} corresponds to the core size perpendicular to the rotational axis of the ellipsoid) and shell SLD (SLD_{shell}) were

simultaneously fitted for all the contrasts available. The structural features of the micelle cross-section were subsequently used to guide the fit of the X-ray data at different concentrations and temperatures. In order to do this, r_{core} was fixed to the value obtained through the previous data co-refinement, as it is assumed that the solvation of the hydrophobic domains will not be greatly affected by changes in concentration or temperature. Therefore, the volume fraction of scatterers (ϕ_{fit}), L_{core}, t_{shell} and SLD_{shell} were determined for these samples.

A polydispersity function (p) was also included for the length of the micelles, whereas the cross-section of the micelle was assumed to be monodisperse. The length distribution is represented using a Schulz function with $p=\sigma/L$, where L is the average length of the micelle and σ is the root-mean-square deviation from L. The width of the distribution is defined by a parameter z such that $z=(1-p^2)/p^2$.[44] As shown in the description in the SasView manual, the function is better behaved with a large N_{pts} and N_{σ}, where N_{pts} is the number of points used to compute the function and N_{σ} defines how far into the tails the distribution is considered in the calculation. For the purposes of the present work and considering the previous indications, the distribution function was parametrized using $N_{pts}=160$ and $N_{\sigma}=15$.

The formation of semiflexible cylinders have been previously reported for amphiphile-based systems, where the morphology of elongated micelles can be described as a worm-like body composed by a succession of rigid sections interconnected by flexible nods.[45-46] Information on the length and flexibility of micelles that fall within that description (elongation > 100 times the radius of the cross-section) were obtained from the combined SANS and SLS data. It should be noted that the Q-range covered by our individual scattering experiments was not sufficient to cover the characteristic features of the scattering curve that contain this information. These data were fitted to a flexible cylinder model, which neglects the internal density distribution of the

micelle (uniform body), but enables the calculation of the contour length of the micelle (L) and the length of the statistical segments or persistence length (l_p, where $2l_p$ is the Kuhn length of the micelle).[45] The elongation of the micelles was subsequently used to refine the fits of the core-shell cylinder model, providing a global model that satisfactorily describes the features of these micelles.

Cryogenic Transmission Electron Microscopy (Cryo-TEM). Small drops (about 4 μL) of the sample were applied on TED PELLA INC F/C 300 mesh Cu grids (Redding, US). The grids had been plasma cleaned in a Blazers SCD004 Sputter coater. The grids were gently blotted with a filter paper and then rapidly frozen in an automatic plunge freezer into liquid ethane (−183 °C) with a Leica EM GP. The vitrified samples were stored in liquid nitrogen (−196 °C) until they were transferred into the microscope using a Fischione Model 2550 Cryo-transfer tomography holder. The grids were examined using a JEOL JEM-2200FS electron microscope (Peabody, US), operated at 200 kV. A TVIPS TemCam-F416 digital camera using Serial EM under low-dose conditions with a 10eV slit was used to record zero-loss images while keeping the working temperature below −175 °C.

Results and discussion

Surfactant adsorption at the air-water interface

For non-ionic surfactants with a given head-group, the CMC generally decreases by an order of magnitude with every two CH2 groups added to the alkyl chain.[47] Based on this relationship and previous studies of shorter-chain congeners (Table 1), the expected CMC of $C_{16}G_2$ is ca 1 μM. In order to determine CMC values, the method used should be sensitive enough to allow for accurate measurements at surfactant concentrations of about an order of magnitude lower. This means that in the present case, accurate measurements should be possible to conduct at sub-

micromolar concentrations, which is experimentally very challenging. More specifically, the main challenge for measuring the surface tension of the systems investigated here is to have a sufficiently large bulk reservoir of surfactant molecules that can adsorb at the interface without depleting the bulk solution. As previously reported, techniques that involve large volumes of solution, such as the Du Noüy ring method, are significantly less affected by bulk depletion.[48] Therefore we have selected such a method for our measurements.

The dependence of the surface tension on concentration is shown in Figure 2. As expected, both α- and β-$C_{16}G_2$ show a decrease in surface tension upon addition of surfactant down to a minimum value, after which the surface tension remains constant even if the surfactant concentration is increased. The intersection between these two regions marks the CMC, above which micelles form in solution. For the surfactants studied here the transition is not sharply defined. The more gradual change of surface tension may be attributed to the presence of small amounts of surface-active contaminants and complicates the definition of the CMC.[49] As presented in the Experimental Section, part of the impurities may be also surface-active components, such as the glucoside surfactant or the other anomeric form of the surfactant, which would cause the effect observed in these results. Taking this into account, we have decided to label the CMC as the intersection between the premicellar region trend and the section where the surface tension levels out to a constant value (See Figure 2). The CMC defined in this way was found to be 1.4±0.1 μM and 2.3±0.2 μM for α- and β-$C_{16}G_2$ respectively, which is in good agreement with the expected value presented above.

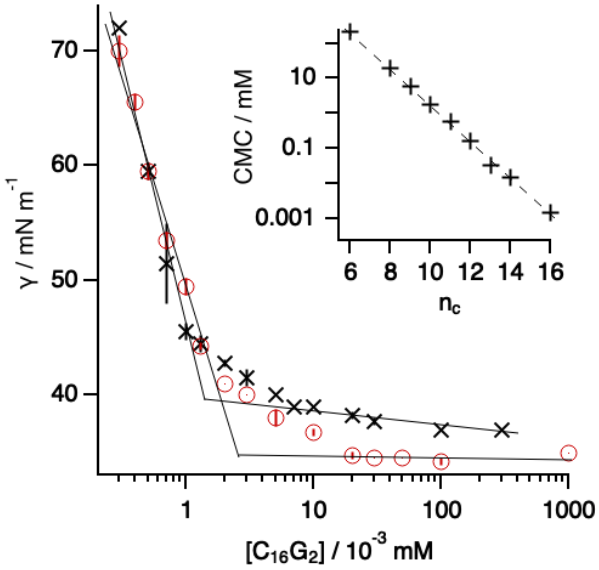

Figure 2 Surface tension of α-$C_{16}G_2$ (×) and β-$C_{16}G_2$ (○) in water (23 ˚C) against the concentration of surfactant. The solid lines represent the pre- and post-micellar trends and help to find the CMC. Inset – CMC trend displays the CMC for a homologous series of β-alkylmaltosides with different carbon tail lengths.[50]

Self-assembly in solution

The self-assembly of α- and β-$C_{16}G_2$ bulk phase as a function of temperature, surfactant concentration and solvent deuteration was studied by means of DLS, SLS, SAXS, SANS and cryo-TEM.

A summary of the DLS results (Figure 3) reveal the presence of micellar aggregates, as inferred by the surface tension data. A complete record of the DLS results for all the concentrations and temperatures can be found in the Supporting Information. It should be noted that the R_H values calculated from DLS using the Stoke-Einstein equation refer to the radius of a sphere with the same diffusion coefficient as the scatterer. As will be discussed below, the self-assembled structures studied here are not spherical. As such, the apparent diffusion coefficient measured by DLS will present contributions from the diffusion of the particle, solvation layer

and trapped solvent, as well as the rotational diffusion of those. Hence, the hydrodynamic radius (R_H) does not constitute an absolute measure of the physical size of the micelles but an apparent dimension that relates to the size and conformation of the micelle. With this in mind, there is still important information that can be extracted from the DLS results about these systems and we have used such a technique to identify trends and morphology transitions that can be later confirmed by means of small-angle scattering.

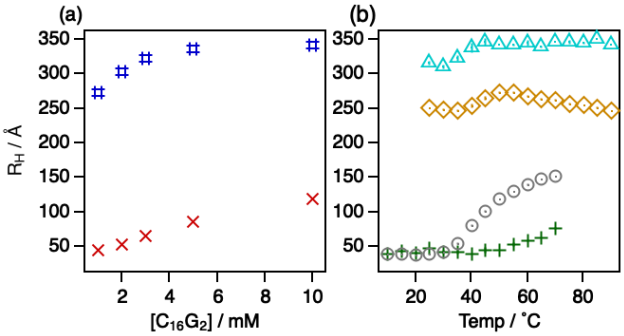

Figure 3 Hydrodynamic radius obtained from Cumulant analysis of DLS data and assuming spherical particles at (a) different surfactant concentrations at 50 ˚C (x – α-$C_{16}G_2$, # – β-$C_{16}G_2$) and (b) temperature (+ – 1 mM α-$C_{16}G_2$, o – 10 mM α-$C_{16}G_2$, ◇ – 1 mM β-$C_{16}G_2$, △ – 10 mM β-$C_{16}G_2$).

Based on the DLS data, the micelles of β-$C_{16}G_2$ (R_H=342±1 Å, 50 ˚C, 10 mM) are considerably larger than those of α-$C_{16}G_2$ (R_H=118±1 Å, 50 ˚C, 10 mM) at all of the conditions measured here. This shows again that there is a major impact of the conformation at the anomeric carbon on the surfactant behavior in solution. Surfactant concentration appears to also affect the size of the micelles in the dilute regime, since the diffusion coefficients suggest a transition from smaller aggregates at low concentrations to larger micelles at higher concentrations (see Figure 3a). For α-$C_{16}G_2$ the apparent R_H changes from 44.1±0.3 Å at 1 mM to 118±1 Å at 10 mM surfactant concentration (50 ˚C). However, this difference is less

pronounced for β-$C_{16}G_2$ as it increases from 273±1 Å at 1 mM to 341±1 Å at 10 mM surfactant concentration (50 ˚C).

The size of the micelles is also influenced by the temperature of the system, and significant differences exist between the two isomeric forms of the surfactant. The α-$C_{16}G_2$ micelles appears to be larger when increasing the temperature, where the largest increase appears when the temperature passes above the Krafft temperature of the surfactant, which has been observed to be between 25 and 35 ˚C. The apparent R_H increases from 39.1±0.1 Å at 25 ˚C to 140±1 Å at 60 ˚C for a 10 mM surfactant solution. The β-$C_{16}G_2$ surfactant forms large structures at low temperature and the variation in size with temperature is less pronounced than in the case of α-$C_{16}G_2$. At low temperatures, close or below the Krafft temperature, micelles show a slightly smaller hydrodynamic radius, 316±1 Å at 25 ˚C, increasing to 345±1 Å at 60 ˚C for the 10 mM sample (see Figure 3b).

As DLS only give an indication of the changes in aggregate size, further structural characterization of the surfactant micelles was performed using SLS, SAXS, SANS, and cryo-TEM. A detailed description of the approach used to fit the data is provided in the Experimental Section. The data and best fits of the applied model to the experimental data are presented in Figure 4. The fitting parameters from the simultaneous fits of SLS, SAXS and SANS are presented in Table 3. A complete record of the fit parameters is included in the Supporting Information.

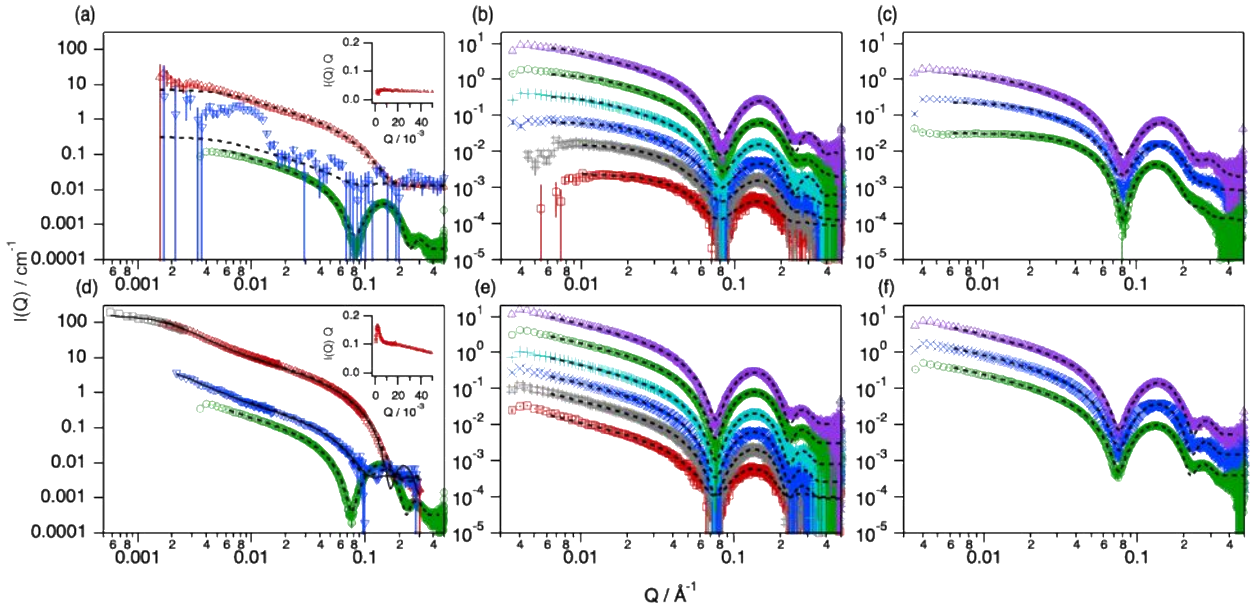

Figure 4 SAXS and SANS data and fits from α- and β-$C_{16}G_2$ micelles in water. (a) SAXS (○) and SANS (△ – α-$C_{16}G_2$ in D_2O, ▽ – α-$C_{16}G_2$ in H_2O) of 10 mM of α-$C_{16}G_2$ at 50 ˚C; (b) SAXS at different surfactant concentrations of α-$C_{16}G_2$ at 50 ˚C (□ – 1 mM, # – 2 mM, × – 3 mM, + – 5 mM, ○ – 10 mM, and △ – 20 mM); (c) SAXS at different temperatures of 10 mM α-$C_{16}G_2$ solutions (○ – 25 ˚C, × – 40 ˚C, and △ – 50 ˚C); (d) SAXS (○), SANS (△ – β-$C_{16}G_2$ in D_2O, ▽ – β-$C_{16}G_2$ in H_2O) and SLS (□) of 18 mM of β-$C_{16}G_2$ at 50 ˚C; (e) SAXS at different surfactant concentrations of β-$C_{16}G_2$ at 50 ˚C (□ – 1 mM, # – 2 mM, × – 3 mM, + – 5 mM, ○ – 10 mM, and △ – 18 mM); (f) SAXS at different temperatures of 10 mM β-$C_{16}G_2$ solutions (○ – 25 ˚C, × – 40 ˚C, and △ – 50 ˚C). The black dashed lines represent the fits using the core-shell ellipsoid or cylinder model, and the flexible cylinder fits are plotted as black solid lines. The insets shown in (a) and (d) present the Holtzer plots (I(Q) Q *vs* Q) of the SANS data for $C_{16}G_2$ in D_2O. Data and fits have been offset in the Y-axis for clarity. Where not seen, error bars are within the markers.

Table 3 Parameters from the combined fit of SAXS and SANS data presented in Figure 4a and d: 10 mM α-$C_{16}G_2$ at 50 ˚C and 18 mM β-$C_{16}G_2$ at 50 ˚C. These results were obtained through the co-refinement of the X-ray and neutron data using the core-shell cylinder and flexible cylinder models.

System	r_{core} / Å	t_{shell} / Å	L_{core} / Å	l_p / Å	φ_{fit} / 10^{-2}	φ_{solv}	N_{agg}	a_0 / Å^2
α-$C_{16}G_2$	14.7±0.3	14.4±0.2	570±10	-	0.73±0.06	0.81±0.01	903±17	
β-$C_{16}G_2$	16.1±0.1	14.9±0.1	6700±400	320±10	1.1±0.1	0.78±0.01	12900±300	53.3±1.8

The exchange of H_2O for D_2O has been previously shown to alter the hydrogen bonding network of the solvent, which in turn affects the micellization of sugar-based surfactants.[26] This effect was further explored by means of DLS and SAXS in the two contrasts used here (see Supporting Information for these results). The difference between H_2O and D_2O in terms of apparent size of α-$C_{16}G_2$ and β-$C_{16}G_2$ micelles can be seen for the conditions investigated here, with larger aggregates being formed in D_2O. Whilst the difference in R_H is rather small for β-$C_{16}G_2$ micelles, the apparent size of α-$C_{16}G_2$ micelles is more significant. This difference may be due to shifts in the transition temperature when exchanging the solvent, which therefore result in shifts in the temperature-induced morphology transition. The influence of the solvent substitution in the headgroup solvation has been evaluated using SAXS. These results have shown that the micelle shell is affected and shows a larger thickness in D_2O, whilst the core of the micelle remains practically unchanged. This implies that the structure of $C_{16}G_2$ micelles vary between the two contrasts measured using the scattering methods presented here, and therefore this effect must be accounted for when determining the structural characteristics of the aggregates. As the solvation effect is predominantly observed at high Q, the results related to this Q-range will be

interpreted through the simultaneous fit of SAXS and SANS data. As the features of the SAXS data at high Q are more pronounced and have a lower experimental error, the fitting will be prone to fit such data, thus minimizing the impact of the isotopic effect from the neutron contrasts. Similarly, information on the elongation of the worm-like micelles is contained in the SLS data (low Q region, data scaled to match the scattering excess of β-$C_{16}G_2$ in D_2O), which is not affected by isotopic substitution as it corresponds to a sample containing surfactant in H_2O. For shorter micelles, where the elongation can be resolved from the X-ray data, no isotope effect is present. Finally, information on the flexibility of the micelle is contained in the intermediate q range, which is covered by the neutron data. As two contrasts were investigated (hydrogenated surfactant in either H_2O or D_2O) the results from the simultaneous fit will be an error-weighted average of those two contrasts.

Therefore, the results obtained through the co-refinement provide an averaged result from both solvents, where this may be more inclined to either the actual values in H_2O or D_2O depending on which technique is mainly driving the fitting. More importantly, the trends observed in the data are the same in H_2O and D_2O, where the beta anomer self-assembles into larger structures than its alpha analogue, and this one undergoes through a sphere-to-rod transition with temperature.

The model used in this study describes a core-shell structure, where the non-solvated hydrophobic core of the micelle is surrounded by a hydrated shell that contains the surfactant headgroups. In order to experimentally probe the different characteristics of worm-like micelles, a wide Q-range is required for the scattering experiments. From the scattering model of a worm-like micelle three regions can be defined: (1) low Q ($Q < 0.004$ Å^{-1}), which is the Guinier region that corresponds to the contour length of the aggregate; (2) intermediate Q (0.004 Å$^{-1} < Q < 0.01$

Å^{-1}) where the oscillation in the data corresponds to the persistence length of the micelle; and (3) high Q (Q > 0.01 Å^{-1}) where a second Guinier region is observed, which corresponds to the cross-section of the micelle and is followed by a decrease in the scattering intensity.[10, 45] The oscillation that corresponds to the persistence length of the micelle can be easily observed in a Holtzer plot (I(Q) Q vs Q). In this plot, the change in scattering cross-section arising from the persistence length is seen as a peak at low Q and, where absent, indicates the lack of significative flexibility. SAXS data also show a strong oscillation at high Q (between *ca.* 0.07 and 0.2 Å^{-1}), which arises from the density correlation core-shell-solvent and can be used, in conjunction with the neutron data, to determine the characteristics of the headgroup region of the micelle (structure and solvation). Therefore, accessing the entire Q-range is of utter importance to build a detailed model of the markedly elongated micelles and this was possible through the combination of SANS, SAXS and SLS.

From the structural parameters obtained through the data analysis, other micelle properties may be calculated. The changes in assembly morphology can, at least in part, be described through the packing parameter.[27] As the hydrophobic moiety of both α- and β-$C_{16}G_2$ is the same, differences in the a_0 relate to changes of packing of the surfactants within the micelles. This parameter can be calculated from the aggregation number of the micelle (N_{agg}) and structural characteristics of the micelle core as follows:

$$N_{agg} = \frac{v_{core}}{v}$$

$$a_0 = \frac{S_{core}}{N_{agg}}$$

where v_{core} is the volume of the core as calculated from the micelle structure, v is the volume of a single tail (same as introduced above for the CPP), and S_{core} is the surface area of the micelle

core. Similarly, the headgroup solvation (as solvent volume fraction at the headgroup shell, φ_{solv}) can be calculated from the fitted SLD of the headgroup shell as:

$$SLD_{shell} = SLD_{hg}(1 - \phi_{solv}) + SDL_{solv}\phi_{solv}$$

where SLD_{shell} corresponds to the fitted SLD of the shell, SLD_{hg} is the calculated SLD of the "anhydrous" headgroup (Table 2), and SLD_{solv} is the calculated SLD of the solvent (Table 2). The variation of these parameters with surfacnat concentration and temperature as derived from the analysis of SAXS data are presented in Figure 5.

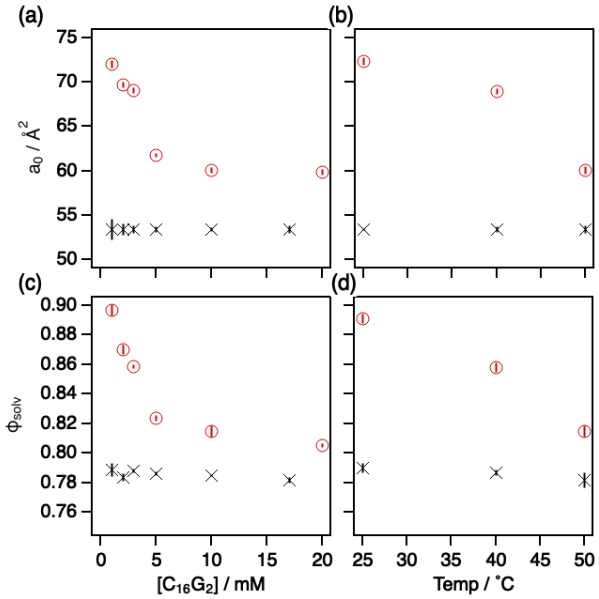

Figure 5 Results derived from the analysis of SAXS data at different surfactant concentration and temperature for: (a, b) Area-per-monomer at the tail-headgroup interface (a_0) and (c, d) solvent volume fraction in the headgroup shell (ϕ_{solv}) for α-$C_{16}G_2$ (○) and β-$C_{16}G_2$ (×).

For each of the systems studied here, the core cross-section is assumed to remain unchanged with temperature and concentration, as well as type of solvent (H_2O and D_2O), as no major variations in the solvent penetration to the hydrophobic region are expected. This value was obtained through the co-refinement of neutron and X-ray data, giving the values of 14.7±0.3 Å

and 16.2±0.1 Å for α- and β-$C_{16}G_2$, respectively. The differences in these values suggest that the β configuration provides a stronger headgroup interaction, which is likely to be a combination of hydrophobic interaction and hydrogen bonding. This type of interaction increases the degree of the headgroup orientation, which in turn also affects the chain packing. We therefore see strong effects of the position of the anomeric carbon, where the core appears to be larger for the β-$C_{16}G_2$ than for the α analog micelles with smaller effects on the thickness of the headgroup region.

As previously shown by DLS, the overall size of the micelles is strongly affected by the configuration of the anomeric carbon in the surfactant headgroup. β-$C_{16}G_2$ micelles were found to be significantly larger than those of α-$C_{16}G_2$, where the difference in size mainly relies on the differences in the length of the micelle as shown by initial analysis of the scattering data. The contour length of the micelle was considered to be polydisperse in the model fitting and is verified in the Cryo-TEM images (See Figure 6). Proper quantification of the polydispersity of the micelle length becomes crucial for the correct evaluation of not only the contour length of the micelle, but also of the micelle flexibility.[10] Previous investigations have shown that for spherical and spheroidal micelles the size distribution is rather narrow, thus the systems are relatively monodisperse. However, Mukerjee predicted that the aggregation number distribution index tends to a value of 2 for large, asymmetric micelles, and therefore the size distribution is wide.[51-52] In order to account for polydispersity effects, a Schulz distribution was used to describe the length distribution of the self-assembled structures. For globular aggregates (elongation ≤ 10 times the radius of the cross-section), the *p* was fixed at a value of 0.1, as these are more likely relatively monodisperse. The *p* value was fixed at 0.7 for the elongated micelles (elongation > 10 times the radius of the cross-section), as this appropriately describes the broad

length distribution of the micelles, as observed in our cryo-TEM images (Figure 6). Using this approach, the contour length (and the persistence length, where present) of the micelles were determined. α-$C_{16}G_2$ forms significantly shorter micelles than β-$C_{16}G_2$, as seen in Table 3. As the only difference between these two surfactants is the configuration of the headgroup, this difference can be attributed to this structural difference. This, in turn, is correlated with the different solvation of the sugar headgroups of two anomers, with the α anomer being more extensively hydrated.

At intermediate Q (around 0.003 $Å^{-1}$), a shoulder is observed in the scattering curves and a peak appears in the Holtzer plots from β-$C_{16}G_2$ micelles (Figure 4d). This arises from the persistence length of the micelle and relates to the flexibility of the assembly (i.e. longer persistence lengths are attributed to higher levels of micelle stiffness).[45] From the simultaneous analysis of SANS and SLS data the contour and persistence length of the micelles could be determined: L=6700±400 Å and l_p=320±10 Å, at 18 mM β-$C_{16}G_2$ concentration, 50 ˚C (L/l_p~21). This value can be directly compared with the reported values for other systems that were determined using a similar approach. Appell *et al.* derived the factors that control the persistence length in micelles and defined two contributions: a steric hindrance, due to geometric constraints, and short-range electrostatic interactions, due to the repulsion between polar headgroups. This investigation showed that a minimum of 90 Å could be found for non-ionic micelles, and this value was around 200 Å for ionic micelles.[53] Using SANS, the anionic surfactant sodium dodecylsulfate (SDS) in the presence of sodium chloride has been reported to form semiflexible aggregates with variable contour and persistence length depending on surfactant and salt concentration.[54] Micelles of the non-ionic surfactant $C_{12}E_5$ and $C_{16}E_6$ have persistence lengths of 120 and 170 Å respectively,[10, 55] and β-$C_{14}G_2$ also forms polymer-like micelles with variable

length and flexibility.[26] The persistence length of β-$C_{16}G_2$ aggregates is similar to that observed for β-$C_{14}G_2$, although the aggregates of the former are larger in general, unlike $C_{12}E_5$ and $C_{16}E_6$ micelles which are reported to be more flexible. This is indicative of the dominant effect of the surfactant headgroup on the flexibility of the aggregates, where the sugar-based surfactants show similar persistence lengths despite the different tail lengths. Similarly, β-$C_{16}G_2$ micelles show increased stiffness compared to the SDS assemblies in the presence of salt, confirming the remarkable rigidity of the sugar-based micelles. The degree of flexibility can also be qualitatively compared to that of polymers or polymer-like systems, where the flexibility for synthetic polymers is often higher (e.g. poly(acrylic) acid) and for biopolymers is lower (e.g. DNA strands).[46] Thus, the flexibility of β-$C_{16}G_2$ micelles is situated between those two non-surfactant-based systems. Although α-$C_{16}G_2$ also forms elongated micelles under certain conditions, the scattering curve did not show any evidence of statistical length. This means that the persistence length of these micelles is on the order of or larger than their contour length.

The surfactant concentration has been found to affect the morphology of the micelles, as seen for other maltoside and ethoxylated surfactants, where increasing the concentration of surfactant promotes elongation of the micelles.[26, 52, 56] The concentration-induced growth of the micelles is remarkably strong for α-$C_{16}G_2$ micelles, where these evolve from globular aggregates at low concentrations (L=85±5 Å, 50 ˚C, 1 mM), to elongated micelles at higher concentrations (L=670±10 Å, 50 ˚C, 20 mM). The β-$C_{16}G_2$ aggregates were found to be more elongated (L=6700±400 Å, 50 ˚C, 18 mM) than the alpha analog in the whole range of concentrations investigated here. Due to the limited experimental Q-range of our SAXS experiments, the contour length of the β-$C_{16}G_2$ micelles could not be resolved for all of the concentrations. Nonetheless, we would expect the elongation of these micelles to be longer than 2000 Å (as the

maximum dimension that can be measured with the current SAXS set up) and of similar dimensions as those of the one we could determine through the combination of all the scattering methods. Therefore, it is seen that the β-$C_{16}G_2$ micelles do not go through a morphology transition at the conditions explored in this work. This assumption is based on the trends observed in the DLS results, were we have seen that changes in elongation of the micelles are not as remarkable as those occurring for the α-$C_{16}G_2$ system.

In a similar fashion to the concentration-induced growth, the elongation of α-$C_{16}G_2$ micelles was found to considerably vary with the temperature of the system, going from rod-like aggregates at 50 ˚C (L=570±10 Å, 10 mM) to shorter, ellipsoidal aggregates at 25 ˚C (L=80±4 Å, 10 mM). On the other hand β-$C_{16}G_2$ micelles appear to show similar elongation in the temperature range explored here. The growth of α-$C_{16}G_2$ micelles with increasing temperature can be explained through an increase in the conformational disorder of the tails and the dehydration of the non-ionic headgroup. The system favors the formation of shorter, highly hydrated micelles at low temperature that then evolve to more elongated micelles at high temperature. This change in morphology, commonly reported as sphere-to-rod transition in micellar systems has been previously reported for non-ionic surfactants from theoretical,[57] experimental,[52] and computational approaches.[58] The absence of this transition in the β-$C_{16}G_2$ micelles with temperature appears to be more complicated to explain. From the results observed here, this distinctive phenomenon must arise from the headgroup interactions, where the β configuration may favor a stronger intermolecular bonding between headgroups. Thus, a change of the spontaneous curvature of the aggregate would require a significant amount of energy to disrupt the arrangement of the headgroups. This may not be compensated by the entropy gain of more flexible tails and thus temperature will not greatly affect the morphology of the micelles.

Interestingly, this behavior is the opposite of what was found for shorter maltoside surfactants. Micelles of β-$C_{10}G_2$ and β-$C_{12}G_2$ shrink to smaller assemblies with increasing temperature, as seen through the combination of SAXS and molecular dynamics simulations.[20] In contrast, neutron and light scattering results showed that β-$C_{14}G_2$ micelles increase monotonically in size with temperature.[26] The change in behavior for the longer surfactant tails may be due to a change in the energy balance between headgroup-headgroup and tail-tail interactions, where the entropic contribution of longer tails may become more significant above a threshold tail length.

As shown in Figure 5, the a_0 for β-$C_{16}G_2$ micelles are smaller than those of α-$C_{16}G_2$. The smaller area (thus larger packing parameter for a given surfactant chain) relates to the formation of longer aggregates, as seen for β-$C_{16}G_2$. As the micelles grow in length, the change in a_0 diminishes asymptotically as it approaches the value for an infinite rod. This means that for very elongated cylinders, such as those of β-$C_{16}G_2$, variations in length result in small changes in a_0 (e.g. a_0(L=4000 Å)=53.5 Å^2; a_0(L=6000 Å)=53.4 Å^2; a_0(L=8000 Å)=53.3 Å^2, as calculated for the cross-section of a β-$C_{16}G_2$ micelle). As the elongation of the micelles could not be resolved for all the conditions measured here and this appears to be in the same order of magnitude as that one we could determine, we have simplified the scenario by assuming that the micelle length will remain constant with concentration and temperature for comparison. Therefore, no change is observed in the trend for a_0 of β-$C_{16}G_2$. The α-$C_{16}G_2$ system, on the other hand, shows significant variations with surfactant concentration and temperature. These changes correlate to the morphology transitions of the assemblies, for which smaller a_0 relate to longer aggregates.

The results for the headgroup solvation show that φ_{solv} for β-$C_{16}G_2$ micelles (~0.78) is consistently lower than that for α-$C_{16}G_2$ micelles (>0.81). This shows that the headgroup hydration is different for these surfactants, which confirms that differences in the morphology

between α- and β-$C_{16}G_2$ micelles arises from a distinct solvation mechanism. Micelles of α-$C_{16}G_2$ present a higher solvation that varies with temperature and surfactant concentration, where larger values relate to higher curvature and thus the formation of shorter micelles. This feature is remarked at temperature below the Krafft point, where α-$C_{16}G_2$ aggregates adopt globular morphologies in what seems to be a kinetically arrested state, where surfactant remains dissolved for several hours before precipitation. A similar behavior in the headgroup solvation has been previously reported for ethylene glycol-linked carbohydrate-based surfactants, where the formation of wormlike micelles is reported to happen at temperatures above 50 ˚C.[59] The hydration of β-$C_{16}G_2$ micelles on the other hand remains rather unchanged with temperature and concentration. The higher solvation levels of α-$C_{16}G_2$ may arise from the packing of the surfactant headgroups, which favors the interaction of the headgroup with water molecules instead of with neighboring headgroups due to the inherent headgroup tilt of the α anomer. The β monomer is characterized by a planar geometry, where the (hydrogen bond and hydrophobic) interactions between headgroups may be more likely. This reduces the available interactions of surfactant headgroups with solvent molecules and prompts the dehydration of the micelle shell, thus reducing the curvature of the aggregate and leading to the formation of elongated micelles. These interactions between headgroups, together with water-headgroup interactions, have been reported for the solvation of glucoside and maltoside surfactants using relaxation NMR.[29] Hydrophobic interactions between headgroups have been also hypothesized to play a role in the solvation of sugar strands.[34-35] In a similar scenario to the hydrogen bond interactions, hydrophobic interactions may be also favored in the β configuration and contribute to the observed dehydration of the headgroup.

Cryo-TEM was used to verify the selection of scattering models to lend support to the results from the scattering data analysis, as it provides direct visualization of the aggregates and can be used to estimate the elongation of the micelles. In agreement with the scattering results, the Cryo-TEM images (Figure 6) show that the β-$C_{16}G_2$ micelles are significantly more elongated than those of α-$C_{16}G_2$, whereas the cross-section of the micelle is similar within the image resolution. The images also reveal the polydisperse character of the micelles, where a distribution of contour and persistence lengths are easily observable. Thus, these results are in good agreement with the models elaborated from the results of the scattering methods.

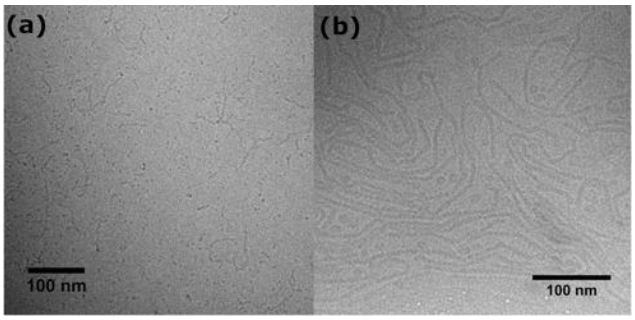

Figure 6 Cryo-TEM images of (a) α-$C_{16}G_2$ 10 mM in H_2O (50 °C prior blotting) and (b) β-$C_{16}G_2$ 10 mM in H_2O (25 °C prior blotting).

Conclusions

The behavior of sugar-based surfactants is of utter importance for fundamental and applied science (e.g. solubilization of membrane proteins) and it is therefore surprising that some fundamental concepts remain rather unexplored and unclear, in particular the effect of surfactant chirality. Here we have explored the effect of the position of the anomeric carbon on the behavior of two long-chain maltoside surfactants, namely α- and β-$C_{16}G_2$, in dilute aqueous solutions. Surface tension measurements were used to determine the CMC of the surfactants, where the two surfactants show different CMCs and α-$C_{16}G_2$ presents a lower value for that.

Structural investigations of micelle morphology by means of scattering techniques and cryo-transmission electron microscopy showed that significant morphological differences are induced when changing in the anomeric carbon. We provide evidence that β-$C_{16}G_2$ forms semiflexible worm-like micelles, which only undergo subtle morphological changes with concentration and temperature. Unlike what was observed for the β isomer of the surfactant, α-$C_{16}G_2$ micelles show a variety of different morphologies. The self-assembly is strongly influenced by the temperature of the system, where a sphere-to-rod transition is observed when increasing the temperature from 25 ˚C to 50 ˚C. A similar transition is observed with surfactant concentration, as the micelles grow longer with increasing the concentration.

The structural changes presented here are therefore induced by the characteristics of the surfactant headgroup, where the only difference between the two surfactants is the configuration of the anomeric carbon. Interestingly, different anomers self-assemble in completely different fashions. This in turn may be explained through the solvation and arrangement of headgroups in the micelles, where the β configuration provides a more efficient packing than the α anomer. This suggests that headgroup-headgroup interactions (hydrogen bond and/or hydrophobic) are more dominant in β-$C_{16}G_2$ micelles than in α-$C_{16}G_2$ micelles, where headgroup-solvent interactions (hydrogen bond) are favored.

The increase of fundamental understanding of these systems, as presented in this study, will assist in the development of sustainable technologies using sugar-based surfactants. As such, the macroscopic response of the system and molecular interactions could be easily tuned through variations in the microstructure of the aggregates and thus in the characteristics of the surfactant molecules.

Associated content

Supporting information. The Supporting Information is available free of charge on the ACS Publication Website.

HPLC chromatograms of the surfactants. Dynamic light scattering and small-angle scattering results. Dynamic light scattering and SAXS of isotope-substituted samples.

Notes

The authors declare no competing financial interest.

Corresponding Author

*E-mail: johan.larsson@fkem1.lu.se

*E-mail: tommy.nylander@fkem1.lu.se

Acknowledgements

This work is based upon experiments performed at the KWS-1 instrument operated by JCNS at the Heinz Maier-Leibnitz Zentrum (MLZ), Garching, Germany. The SANS experiments on Sans2d at the ISIS Pulsed Neutron and Muon Source were supported by a beamtime allocation from the Science and Technology Facilities Council. The SAXS experiments were performed on beamline BM29 at the European Synchrotron Radiation Facility (ESRF), Grenoble, France. We are grateful to Martha Brennich at the ESRF for providing assistance in using the beamline. We would like to thank Prof. Karin Schillén for the fruitful discussions on light scattering and Dr. Stephen King for the constructive input into micelle polydispersity. This work benefited from the use of the SasView application, originally developed under NSF award DMR-0520547. SasView contains code developed with funding from the European Union's Horizon 2020 research and innovation programme under the SINE2020 project, grant agreement No 654000. The National Center for High Resolution Electron Microscopy, Lund University, is gratefully acknowledged

for providing experimental resources. We would also like to thank Anna Carnerup at the Physical Chemistry Department, Lund University, for the support provided during the Cryo-TEM measurements. The authors are also thankful to Swedish Research Council Formas (Grant 2015-666) for the funding for J.L. The research in this study was performed with financial support from Vinnova - Swedish Governmental Agency for Innovation Systems within the NextBioForm Competence Centre.

References

1. Hill, K.; Rhode, O., Sugar-based surfactants for consumer products and technical applications. *Lipid / Fett* **1999,** *101* (1), 25-33.
2. Foley, P.; Kermanshahi pour, A.; Beach, E. S.; Zimmerman, J. B., Derivation and synthesis of renewable surfactants. *Chemical Society Reviews* **2012,** *41* (4), 1499-1518.
3. Chatterjee, C.; Pong, F.; Sen, A., Chemical conversion pathways for carbohydrates. *Green Chemistry* **2015,** *17* (1), 40-71.
4. Balzer, D.; Lüders, H., *Nonionic surfactants : alkyl polyglucosides*. Marcel Dekker: New York, 2000.
5. Seddon, A. M.; Curnow, P.; Booth, P. J., Membrane proteins, lipids and detergents: not just a soap opera. *Biochimica et Biophysica Acta (BBA) - Biomembranes* **2004,** *1666* (1), 105-117.
6. Strey, R.; Schomäcker, R.; Roux, D.; Nallet, F.; Olsson, U., Dilute lamellar and L3 phases in the binary water–C12E5 system. *Journal of the Chemical Society, Faraday Transactions* **1990,** *86* (12), 2253-2261.
7. Nilsson, P. G.; Wennerström, H.; Lindman, B., Structure of micellar solutions of nonionic surfactants. Nuclear magnetic resonance self-diffusion and proton relaxation studies of poly (ethylene oxide) alkyl ethers. *The Journal of Physical Chemistry* **1983,** *87* (8), 1377-1385.
8. Mitchell, D. J.; Tiddy, G. J. T.; Waring, L.; Bostock, T.; McDonald, M. P., Phase behaviour of polyoxyethylene surfactants with water. Mesophase structures and partial miscibility (cloud points). *Journal of the Chemical Society, Faraday Transactions 1: Physical Chemistry in Condensed Phases* **1983,** *79* (4), 975-1000.
9. Patist, A.; Bhagwat, S. S.; Penfield, K. W.; Aikens, P.; Shah, D. O., On the measurement of critical micelle concentrations of pure and technical-grade nonionic surfactants. *Journal of Surfactants and Detergents* **2000,** *3* (1), 53-58.
10. Jerke, G.; Pedersen, J. S.; Egelhaaf, S. U.; Schurtenberger, P., Flexibility of Charged and Uncharged Polymer-like Micelles. *Langmuir* **1998,** *14* (21), 6013-6024.
11. Tiberg, F.; Joensson, B.; Tang, J.-a.; Lindman, B., Ellipsometry Studies of the Self-Assembly of Nonionic Surfactants at the Silica-Water Interface: Equilibrium Aspects. *Langmuir* **1994,** *10* (7), 2294-2300.

12. Zhang, R.; Marone, P. A.; Thiyagarajan, P.; Tiede, D. M., Structure and Molecular Fluctuations of n-Alkyl-β-d-glucopyranoside Micelles Determined by X-ray and Neutron Scattering. *Langmuir* **1999,** *15* (22), 7510-7519.
13. Lipfert, J.; Columbus, L.; Chu, V. B.; Lesley, S. A.; Doniach, S., Size and Shape of Detergent Micelles Determined by Small-Angle X-ray Scattering. *The Journal of Physical Chemistry B* **2007,** *111* (43), 12427-12438.
14. Nilsson, F.; Söderman, O.; Johansson, I., Four Different C8G1 Alkylglucosides. Anomeric Effects and the Influence of Straight vs Branched Hydrocarbon Chains. *Journal of Colloid and Interface Science* **1998,** *203*, 131-139.
15. Nilsson, F.; Söderman, O.; Johansson, I., Physical−Chemical Properties of the n-Octyl β-d-Glucoside/Water System. A Phase Diagram, Self-Diffusion NMR, and SAXS Study. *Langmuir* **1996,** *12* (4), 902-908.
16. Ericsson, C. A.; Söderman, O.; Garamus, V. M.; Bergström, M.; Ulvenlund, S., Effects of Temperature, Salt, and Deuterium Oxide on the Self-Aggregation of Alkylglycosides in Dilute Solution. 1. n-Nonyl-β-d-glucoside. *Langmuir* **2004,** *20* (4), 1401-1408.
17. Nilsson, F.; Söderman, O.; Hansson, P.; Johansson, I., Physical−Chemical Properties of C9G1 and C10G1 β-Alkylglucosides. Phase Diagrams and Aggregate Size/Structure. *Langmuir* **1998,** *14* (15), 4050-4058.
18. He; Garamus, V. M.; Funari, S. S.; Malfois, M.; Willumeit, R.; Niemeyer, B., Comparison of Small-Angle Scattering Methods for the Structural Analysis of Octyl-β-maltopyranoside Micelles. *The Journal of Physical Chemistry B* **2002,** *106* (31), 7596-7604.
19. Alpes, H.; Allmann, K.; Plattner, H.; Reichert, J.; Rick, R.; Schulz, S., Formation of large unilamellar vesicles using alkyl maltoside detergents. *BBA - Biomembranes* **1986,** *862* (2), 294-302.
20. Ivanović, M. T.; Bruetzel, L. K.; Lipfert, J.; Hub, J. S., Temperature-Dependent Atomic Models of Detergent Micelles Refined against Small-Angle X-Ray Scattering Data. *Angewandte Chemie International Edition* **2018,** *57* (20), 5635-5639.
21. Dupuy, C.; Auvray, X.; Petipas, C.; Rico-Lattes, I.; Lattes, A., Anomeric Effects on the Structure of Micelles of Alkyl Maltosides in Water. *Langmuir* **1997,** *13* (15), 3965-3967.
22. Jensen, G. V.; Lund, R.; Gummel, J.; Monkenbusch, M.; Narayanan, T.; Pedersen, J. S., Direct Observation of the Formation of Surfactant Micelles under Nonisothermal Conditions by Synchrotron SAXS. *Journal of the American Chemical Society* **2013,** *135* (19), 7214-7222.
23. Putra, E. G. R.; Ikram, A., A 36m SANS BATAN spectrometer (SMARTer): Probing n-dodecyl-β-d-maltoside micelles structures by a contrast variation. *Nuclear Instruments and Methods in Physics Research Section A: Accelerators, Spectrometers, Detectors and Associated Equipment* **2009,** *600* (1), 288-290.
24. Bäverbäck, P.; Oliveira, C. L. P.; Garamus, V. M.; Varga, I.; Claesson, P. M.; Pedersen, J., Structural Properties of β-Dodecylmaltoside and C12E6 Mixed Micelles. *Langmuir* **2009,** *25* (13), 7296-7303.
25. Cecutti, C.; Focher, B.; Perly, B.; Zemb, T., Glycolipid self-assembly: micellar structure. *Langmuir* **1991,** *7* (11), 2580-2585.
26. Ericsson, C. A.; Söderman, O.; Garamus, V. M.; Bergström, M.; Ulvenlund, S., Effects of temperature, salt, and deuterium oxide on the self-aggregation of alkylglycosides in dilute solution. 2. n-Tetradecyl-beta-D-maltoside. *Langmuir: The ACS Journal Of Surfaces And Colloids* **2005,** *21* (4), 1507-1515.

27. Israelachvili, J. N.; Mitchell, D. J.; Ninham, B. W., Theory of self-assembly of hydrocarbon amphiphiles into micelles and bilayers. *Journal of the Chemical Society, Faraday Transactions 2: Molecular and Chemical Physics* **1976,** *72* (0), 1525-1568.
28. Boyd, B. J.; Drummond, C. J.; Krodkiewska, I.; Grieser, F., How Chain Length, Headgroup Polymerization, and Anomeric Configuration Govern the Thermotropic and Lyotropic Liquid Crystalline Phase Behavior and the Air−Water Interfacial Adsorption of Glucose-Based Surfactants. *Langmuir* **2000,** *16* (19), 7359-7367.
29. Cardoso, M. V. C.; Sabadini, E., Before and Beyond the Micellization of n-Alkyl Glycosides. A Water-1H NMR Relaxation Study. *Langmuir* **2013,** *29* (51), 15778-15786.
30. Ranieri, D.; Preisig, N.; Stubenrauch, C., On the Influence of Intersurfactant H-Bonds on Foam Stability: A Study with Technical Grade Surfactants. *Tenside Surfactants Detergents* **2018,** *55* (1), 6-16.
31. Whiddon, C.; Söderman, O., Unusually Large Deuterium Isotope Effects in the Phase Diagram of a Mixed Alkylglucoside Surfactant/Water System. *Langmuir* **2001,** *17* (6), 1803-1806.
32. Szejtli, J., Introduction and General Overview of Cyclodextrin Chemistry. *Chemical Reviews* **1998,** *98* (5), 1743-1754.
33. Funasaki, N.; Ishikawa, S.; Neya, S., Advances in physical chemistry and pharmaceutical applications of cyclodextrins. *Pure and Applied Chemistry* **2008,** *80* (7), 1511-1524.
34. Alves, L.; Medronho, B. F.; Antunes, F. E.; Romano, A.; Miguel, M. G.; Lindman, B., On the role of hydrophobic interactions in cellulose dissolution and regeneration: Colloidal aggregates and molecular solutions. *Colloids and Surfaces A: Physicochemical and Engineering Aspects* **2015,** *483*, 257-263.
35. Glasser, W. G.; Atalla, R. H.; Blackwell, J.; Malcolm Brown, R.; Burchard, W.; French, A. D.; Klemm, D. O.; Nishiyama, Y., About the structure of cellulose: debating the Lindman hypothesis. *Cellulose* **2012,** *19* (3), 589-598.
36. Pernot, P.; Round, A.; Barrett, R.; De Maria Antolinos, A.; Gobbo, A.; Gordon, E.; Huet, J.; Kieffer, J.; Lentini, M.; Mattenet, M.; Morawe, C.; Mueller-Dieckmann, C.; Ohlsson, S.; Schmid, W.; Surr, J.; Theveneau, P.; Zerrad, L.; McSweeney, S., Upgraded ESRF BM29 beamline for SAXS on macromolecules in solution. *Journal of Synchrotron Radiation* **2013,** *20* (4), 660-664.
37. Orthaber, D.; Bergmann, A.; Glatter, O., SAXS experiments on absolute scale with Kratky systems using water as a secondary standard. *Journal of Applied Crystallography* **2000,** *33* (2), 218-225.
38. Frielinghaus, H.; Feoktystov, A.; Berts, I.; Mangiapia, G., KWS-1: Small-angle scattering diffractometer. *Journal of large-scale research facilities JLSRF* **2015,** *1*, 28.
39. Heenan, R. K.; Rogers, S. E.; Turner, D.; Terry, A. E.; Treadgold, J.; King, S. M., Small Angle Neutron Scattering Using Sans2d. *Neutron News* **2011,** *22* (2), 19-21.
40. Feoktystov, A. V.; Frielinghaus, H.; Di, Z.; Jaksch, S.; Pipich, V.; Appavou, M.-S.; Babcock, E.; Hanslik, R.; Engels, R.; Kemmerling, G.; Kleines, H.; Ioffe, A.; Richter, D.; Bruckel, T., KWS-1 high-resolution small-angle neutron scattering instrument at JCNS: current state. *Journal of Applied Crystallography* **2015,** *48* (1), 61-70.
41. Doucet, M.; Cho, J. H.; Alina, G.; Bakker, J.; Bouwman, W.; Butler, P.; Campbell, K.; Gonzales, M.; Heenan, R.; Jackson, A.; Juhas, P.; King, S.; Kienzle, P.; Krzywon, J.; Markvardsen, A.; Nielsen, T.; O'Driscoll, L.; Potrzebowski, W.; Ferraz Leal, R.; Richter, T.; Rozycko, P.; Washington, A. *SasView version 4.1*, 2017.

42. Tanford, C., Micelle shape and size. *The Journal of Physical Chemistry* **1972,** *76* (21), 3020-3024.
43. Pedersen, J. S., Analysis of small-angle scattering data from colloids and polymer solutions: modeling and least-squares fitting. *Advances in Colloid and Interface Science* **1997,** *70*, 171-210.
44. Kotlarchyk, M.; Chen, S. H., Analysis of small angle neutron scattering spectra from polydisperse interacting colloids. *The Journal of Chemical Physics* **1983,** *79* (5), 2461-2469.
45. Pedersen, J. S.; Schurtenberger, P., Scattering Functions of Semiflexible Polymers with and without Excluded Volume Effects. *Macromolecules* **1996,** *29* (23), 7602-7612.
46. Dreiss, C. A., Wormlike micelles: where do we stand? Recent developments, linear rheology and scattering techniques. *Soft Matter* **2007,** *3* (8), 956-970.
47. Mattei, M.; Kontogeorgis, G. M.; Gani, R., Modeling of the Critical Micelle Concentration (CMC) of Nonionic Surfactants with an Extended Group-Contribution Method. *Industrial & Engineering Chemistry Research* **2013,** *52* (34), 12236-12246.
48. Kairaliyeva, T.; Aksenenko, E. V.; Mucic, N.; Makievski, A. V.; Fainerman, V. B.; Miller, R., Surface Tension and Adsorption Studies by Drop Profile Analysis Tensiometry. *Journal of Surfactants and Detergents* **2017,** *20* (6), 1225-1241.
49. Elworthy, P. H.; Mysels, K. J., The surface tension of sodium dodecylsulfate solutions and the phase separation model of micelle formation. *Journal of Colloid and Interface Science* **1966,** *21* (3), 331-347.
50. Anatrace https://www.anatrace.com/ (accessed 15-11-2018).
51. Mukerjee, P., Size distribution of small and large micelles. Multiple equilibrium analysis. *The Journal of Physical Chemistry* **1972,** *76* (4), 565-570.
52. Glatter, O.; Fritz, G.; Lindner, H.; Brunner-Popela, J.; Mittelbach, R.; Strey, R.; Egelhaaf, S. U., Nonionic Micelles near the Critical Point: Micellar Growth and Attractive Interaction. *Langmuir* **2000,** *16* (23), 8692-8701.
53. Appell, J.; Porte, G.; Poggi, Y., Quantitative estimate of the orientational persistence length of flexible elongated micelles of cetylpyridinium bromide. *Journal of Colloid and Interface Science* **1982,** *87* (2), 492-499.
54. Magid, L. J.; Li, Z.; Butler, P. D., Flexibility of Elongated Sodium Dodecyl Sulfate Micelles in Aqueous Sodium Chloride: A Small-Angle Neutron Scattering Study. *Langmuir* **2000,** *16* (26), 10028-10036.
55. Kwon, S. Y., Length Control in Rigid Cylindrical Nanoassembly by Tuning Molecular Interactions in Aqueous Solutions. *Langmuir* **2008,** *24* (19), 10674-10679.
56. Schurtenberger, P.; Cavaco, C.; Tiberg, F.; Regev, O., Enormous Concentration-Induced Growth of Polymer-like Micelles. *Langmuir* **1996,** *12* (12), 2894-2899.
57. Puvvada, S.; Blankschtein, D., Molecular-thermodynamic approach to predict micellization, phase behavior and phase separation of micellar solutions. I. Application to nonionic surfactants. *The Journal of Chemical Physics* **1990,** *92* (6), 3710-3724.
58. Velinova, M.; Sengupta, D.; Tadjer, A. V.; Marrink, S.-J., Sphere-to-rod transitions of nonionic surfactant micelles in aqueous solution modeled by molecular dynamics simulations. *Langmuir* **2011,** *27* (23), 14071-14077.
59. Moore, J. E.; McCoy, T. M.; de Campo, L.; Sokolova, A. V.; Garvey, C. J.; Pearson, G.; Wilkinson, B. L.; Tabor, R. F., Wormlike micelle formation of novel alkyl-tri(ethylene glycol)-glucoside carbohydrate surfactants: Structure–function relationships and rheology. *Journal of Colloid and Interface Science* **2018,** *529*, 464-475.